Journal of Materials Chemistry C

PAPER

View Article Online
View Journal | View Issue

Cite this: J. Mater. Chem. C, 2017, 5, 11885

Photovoltage as a quantitative probe of carrier generation and recombination in organic photovoltaic cells†

Tao Zhang and Russell J. Holmes *

Received 17th September 2017,
Accepted 30th October 2017

DOI: 10.1039/c7tc04246a

rsc.li/materials-c

Photoconversion in organic photovoltaic cells (OPVs) is limited by carrier recombination that frustrates charge collection at the electrodes. Consequently, identification of the dominant recombination mechanisms is critical to inform device design for improved performance. This analysis is complicated by the need to have a quantitative measure of carrier generation. Here, we demonstrate a photovoltage-based technique to directly investigate the generation of charge carriers in OPVs. This technique allows illuminated current losses to both geminate and non-geminate recombination to be directly quantified as a function of voltage. While broadly applicable, here the technique is demonstrated on OPVs based on the donor–acceptor pairings of 2-((7-(4-*N*,*N*-ditolylaminophenylen-1-yl)benzo[c][1,2,5]thiadiazol-4-yl)-methylene)malononitrile (DTDCPB)-C_{60} and copper phthalocyanine (CuPc)-C_{60}. Both structures are limited by geminate recombination at short-circuit and under reverse bias. Under forward bias, the severity of non-geminate recombination depends on both materials selection and device architecture. Consequently, this technique quantitatively casts changes in performance with choice of OPV architecture in terms of the relative roles of geminate and non-geminate recombination.

Introduction

Improvements in the performance of organic photovoltaic cells (OPVs) have been driven by efforts in molecular design, optimization of film processing, and enhancements in device architecture.[1–7] This has permitted devices based on both small molecule and polymer active materials to exceed power conversion efficiencies (η_P) of 10%.[8–12] As most high efficiency devices employ the bulk heterojunction (BHJ) architecture to ensure efficient exciton harvesting, charge carrier losses due to recombination are the primary bottleneck to further increases in performance.[13]

During photoconversion, intermolecular charge transfer (CT) states form when excitons are dissociated at a donor–acceptor (D–A) interface. These CT states may either dissociate into free charge carriers (mobile polarons) or, recombine (geminate recombination). If the CT state is dissociated, the generated charge carriers must be collected at the electrodes prior to recombination with another free carrier (non-geminate recombination).[13] Previous work has shown that both geminate and non-geminate recombination are voltage dependent and can limit the illuminated current under forward bias, thereby limiting the short-circuit current (I_{SC}), open-circuit voltage (V_{OC}) and fill factor (FF).[14–17] It is thus critical to develop a deeper and more quantitative understanding of how various recombination mechanisms dominate device performance in order to better guide activities in materials and device engineering.[13]

Fig. 1a shows the component processes of photoconversion in an OPV. These processes can be quantified as current using:

$$I_{Max} - I_{GR} - I_{NGR} = I_{Gen} - I_{NGR} = I_{Illum} \quad (1)$$

In eqn (1), I_{Max} is the maximum achievable current in the absence of all charge carrier recombination, determined by the generation rate and the efficiency of exciton dissociation at the D–A interface. I_{GR} and I_{NGR} are current losses due to geminate and non-geminate recombination, respectively. On the right of eqn (1), I_{Illum} is the final collected current at the electrodes, experimentally measured from device current–voltage (I–V) characteristics under illumination. Charge collection can thus be separated into two component processes, the separation

Department of Chemical Engineering and Materials Science, University of Minnesota, Minneapolis, MN 55455, USA. E-mail: rholmes@umn.edu

† Electronic supplementary information (ESI) available: Comparison between timescales for charge extraction and open-circuit voltage decay, carrier lifetime, additional plots of carrier rise and decay, intensity dependence of short-circuit current for DTDCPB-C_{60} BHJ OPVs, intensity dependent CE for various operating voltages, recreation of intensity dependent I_{Illum}, charge collection efficiency of DTDCPB-C_{60} BHJ OPVs using reverse bias external quantum efficiency measurements, comparison between I_{Gen} and $I_{Illum} - I_{Dark}$ difference, bias dependent charge separation efficiencies of DTDCPB-C_{60} BHJ and PMHJ OPVs, pump LED spectra, device performance under 1 Sun illumination. See DOI: 10.1039/c7tc04246a

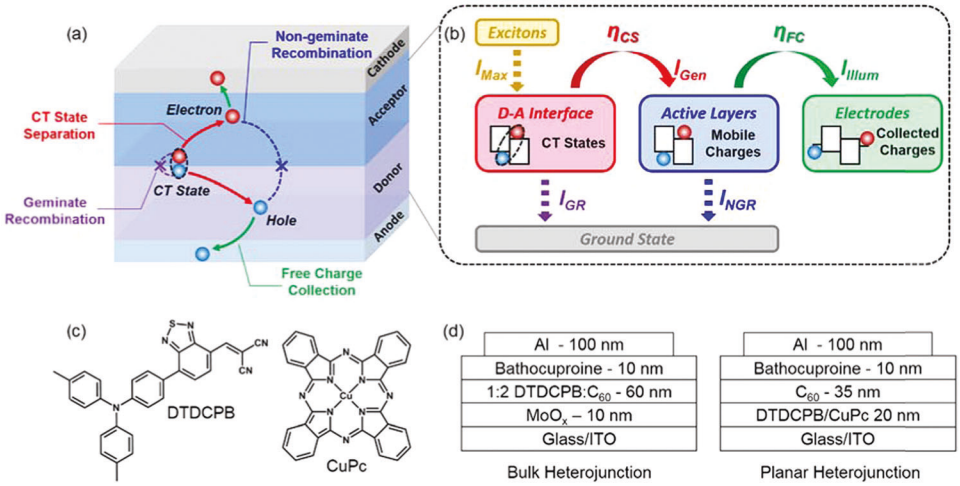

Fig. 1 (a) Geminate recombination (GR), charge transfer (CT) state separation (free charge generation), non-geminate recombination (NGR) and free charge collection processes in a donor–acceptor OPV during photoconversion. (b) The currents that represent the component processes of photoconversion discussed in the text. (c) Molecular structures of DTDCPB and CuPc. (d) Device architectures of interest in this work.

of CT states and the collection of free charges, with an efficiency:

$$\eta_{CC} = \eta_{CS}\eta_{FC} = \left(\frac{I_{Gen}}{I_{Max}}\right)\left(\frac{I_{Illum}}{I_{Gen}}\right) = \left(\frac{I_{Illum}}{I_{Max}}\right) \qquad (2)$$

In eqn (2), η_{CC} is the overall charge collection efficiency, the ratio of collected free charges to generated CT states. The component efficiencies, the charge separation efficiency (η_{CS}) and the free charge collection efficiency (η_{FC}), are the ratio of I_{Gen} to I_{Max} and I_{Illum} to I_{Gen}, respectively (Fig. 1b). Thus, geminate and non-geminate losses can be quantitatively examined with knowledge of η_{CS} and η_{FC}.

Previously, a variety of approaches have been used to measure I_{Max} in order to deduce the overall charge carrier recombination loss from the difference between I_{Max} and I_{Illum} (I–V characteristics).[18–21] Nonetheless, experimentally determining the efficiency of CT state dissociation remains an area of active research as it is crucial for decoupling geminate and non-geminate recombination.[16,22,23] The I_{Gen} in an OPV is typically extracted as the 'photocurrent', which is the difference between the illuminated current and the dark current.[24] This simple calculation assumes that the current to non-geminate recombination under illumination is the same as it is in the dark.[25,26] This assumption is however not necessarily true as previous work has shown that non-geminate recombination can be light intensity dependent.[27] Other techniques have sought to measure the voltage dependent I_{Gen}, including transient absorption spectroscopy (TAS) and time delayed collection field (TDCF) measurements.[16,22,23] However, these techniques require the use of a high power laser rather than a solar simulated light source. It therefore can be challenging to translate results into a value of the current comparable to solar simulated I–V characteristics.[16,22,28,29] This complicates the extraction of I_{Gen}, a decoupling that is essential for deeper examinations of charge carrier recombination in OPVs.

Here, a photovoltage-based technique is used to directly measure I_{Gen}. In this measurement, an OPV is held at open-circuit so that non-geminate recombination within the device is

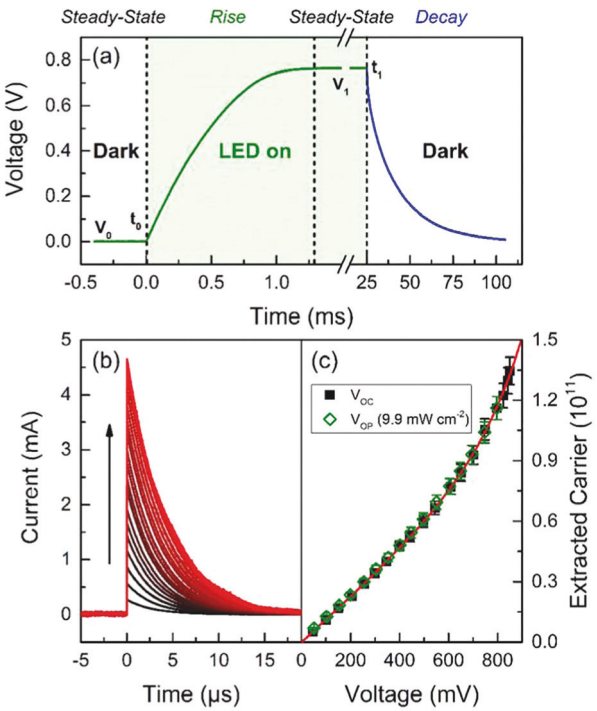

Fig. 2 (a) The photovoltage rise and decay of the DTDCPB-C_{60} BHJ in Fig. 1d caused by green LED illumination (9.9 mW cm^{-2}) turned on from t = 0 ms to 25 ms in the absence of background illumination. (b) Current transients obtained by switching the device in (a) from steady state open-circuit to short-circuit. The steady state voltage is varied from 47.0 mV to 851.0 mV. (c) The number of extracted carriers as a function of open-circuit voltage (V_{OC}) and operating voltage (V_{OP}) derived by integrating current transients with respect to time. The solid red line is the sum of a linear fit for data up to 300 mV and an exponential fit.

the only pathway for consuming free charge carriers. In the most general version of this technique, the OPV is initially under steady-state illumination leading to a corresponding open-circuit voltage (V_0). At a later time t_0, the light intensity is increased and the resulting transient photovoltage (TPV) rise is recorded (a typical TPV trace is shown in Fig. 2a). The TPV rise can be quantitatively translated into an increase in the number of charge carriers (n) in the device when a general relationship between open-circuit voltage and carrier number is separately known. Here, charge extraction (CE) methods are used to experimentally determine this relationship. With knowledge of the number of charge carriers stored in the device as a function of time, the charge accumulation rate can be estimated from the slope of carrier number rise. Close to t_0, free carrier recombination losses are negligible when the timescale is much shorter than the free carrier lifetime (τ).[30] Thus a linear increase in charge carrier number will be observed and the I_{Gen} at V_0 can be readily extracted from the accumulation rate of charge carriers. The background illumination can be varied in order to vary V_0 and extract I_{Gen} as a function of open-circuit voltage. As open-circuit and actual operating conditions can correspond to a slightly different number of carriers in the device at a given voltage, a second CE measurement is carried out to determine the relationship between operating voltage (V_{OP}) and n, which allows V_0 to be converted to V_{OP}.[31] Comparing the extracted I_{Gen} (V_{OP}) with commonly measured current–voltage (I–V) characteristics, we are able to quantify illuminated current losses to both geminate and non-geminate recombination as a function of voltage. As TPV is often used to determine charge carrier lifetimes and the voltage dependence of non-geminate recombination, we are also able to measure I_{NGR} directly to check the validity of this technique.

Experimental

Organic photovoltaic cells were fabricated using pre-patterned indium-tin-oxide (ITO)-coated glass substrates with a sheet resistance of 15 $\Omega\ \square^{-1}$. Substrates were cleaned in tergitol solution and in organic solvents and treated in UV-ozone ambient for 10 minutes prior to thin film deposition. All layers were deposited at room temperature by high vacuum thermal evaporation at a pressure of $<8 \times 10^{-7}$ Torr. In BHJ devices, a 10 nm-thick layer of MoO_x was deposited at 0.05 nm s^{-1} on ITO as an anode buffer layer.[44] Mixed organic layers were prepared *via* co-deposition from two sources at a total rate of 0.2 nm s^{-1}. All devices are capped with a 10 nm-thick exciton blocking layer (EBL) of bathocuproine (BCP) and a 100 nm-thick Al cathode. The active area of the obtained device is 0.25 cm^2. For this study, 2-((7-(4-*N*,*N*-ditolylaminophenylen-1-yl)benzo[*c*][1,2,5]thiadiazol-4-yl)methylene)malononitrile (DTDCPB) ($\approx$97%) was obtained from Sigma-Aldrich,[3] C_{60} ($\approx$99%) was obtained from MER Corporation, MoO_3 (99.5%) and BCP (98%) were obtained from Alfa Aesar. All materials were used as received without further purification. Transient photovoltage and charge extraction measurements were conducted per previously published methods (illumination area: 0.0176 cm^2).[30,31] The spectra of green and blue LEDs used in this work can be found in ESI.† Current density–voltage characteristics were measured in air ambient with an Agilent 4155C parameter analyzer. Photocurrent under bias was measured using a Stanford Research Systems SR810 lock-in amplifier and a SR570 current preamplifier. External quantum efficiency measurements were performed under illumination from a 300 W Xe lamp coupled to a monochromator and chopped with a SR540 optical shopper. All film thicknesses and optical constants were measured with a J. A. Woollam spectroscopic ellipsometer (fit using a Cauchy model).

Results and discussion

To demonstrate the photovoltage-based technique, we first quantify the illuminated current losses from geminate and non-geminate recombination for a small molecule BHJ OPV based on the high efficiency D–A pairing of DTDCPB-C_{60}.[3,32,33] Two planar heterojunction (PHJ) OPVs based on the D–A pairings of DTDCPB-C_{60} and copper phthalocyanine (CuPc)-C_{60} are also examined. Fig. 1c and d shows the electron donors and device architectures of interest for this study. The performance of these devices is shown in Table S1 (ESI†).

Fig. 2a shows a representative TPV response for a DTDCPB-C_{60} BHJ OPV under illumination by a green LED (λ_{peak} = 530 nm, intensity: 9.9 mW cm^{-2}) turned on at $t = t_0$ (0 μs) and turned off at $t = t_1$ (25 ms). Prior to t_0, the voltage (V_0) is constant as steady-state is reached with no background illumination. Under illumination, the photovoltage increases with a decreasing slope until a new steady-state voltage (V_1) is reached. Only the first few microseconds of the TPV rise are used for the extraction of I_{Gen} to avoid potential non-geminate losses, consistent with previous work.[30]

To translate photovoltage transients into a measure of charge carrier accumulation, CE methods are used to connect photovoltage and the number of charge carriers stored within the device. In the CE measurement, OPVs are first illuminated at open-circuit to reach steady-state. This is followed by a rapid switching of the device to short-circuit, with the resulting current transient recorded. Fig. 2b shows the current transients (from starting voltages ranging from 47.0 mV to 851.0 mV) recorded for the DTDCPB-C_{60} BHJ in Fig. 1d. The number of stored charge carriers is the integral of each current transient, and plotted *versus* the initial steady-state V_{OC} (Fig. 2c). Although non-geminate recombination may take place during the CE experiment and lead to an underestimate in the number of carriers present in the device, the much shorter time required to complete the CE *versus* the photovoltage decay at open-circuit suggests that only a negligible fraction of carriers recombine within the device rather than through the outside circuit (Fig. S1, ESI†). It should be noted that the extracted carriers include those stored at both electrodes and in the active layers. In many previous works studying non-geminate recombination, carriers stored at the electrodes (increase linearly with voltage) are often subtracted from CE results in order to

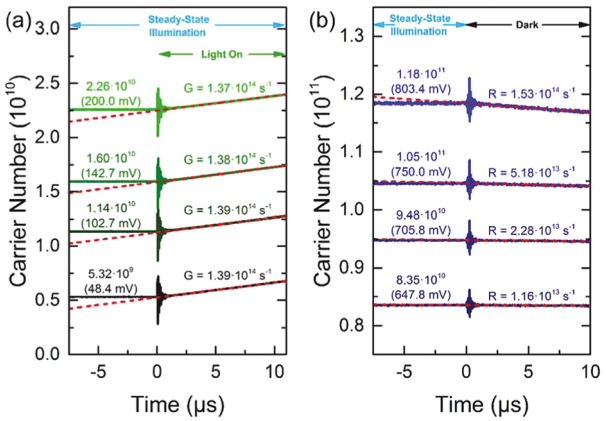

Fig. 3 (a) Representative plots of charge carriers stored within the device in Fig. 1d *versus* time for measurement of carrier generation rate (G). (b) Representative plots of carrier decay for measurement of carrier recombination rate (R). The rates are approximated as the slope of linear rise/decay region. A variable background blue LED illumination is used to set the target steady-state carrier number and corresponding V_{OP} (in the brackets) for measurement.

isolate carriers stored in the active layer (increase exponentially with voltage).[15,16,27]

By translating TPV into charge carriers, carrier number as a function of time can be plotted. Fig. 3a shows four representative plots of carrier number *versus* time for the DTDCPB-C_{60} BHJ in Fig. 1d. A second blue LED (λ_{peak} = 455 nm) provides background illumination and is used to vary the steady-state carrier number n_0. As the green LED illumination is mostly absorbed by DTDCPB, a blue LED (mostly absorbed by C_{60}) is chosen to avoid a significant change in exciton generation for the donor. The value of the initial steady-state carrier number (n_0) is taken as the average value before t = 0 μs ($n_0 = 5.32 \times 10^9$, 1.14×10^{10}, 1.60×10^{10}, 2.26×10^{10} in Fig. 3a). For a very short time after t_0, the increase in n is not significant, we can therefore assume that the changes in carrier generation rates and carrier lifetime are not significant. The accumulation rate $\left(\frac{dn}{dt}\right)$ after t_0 is then given as:

$$\frac{dn}{dt} = (G_{BG} + G) - \left(R + \frac{n - n_0}{\tau}\right) = G - \frac{n - n_0}{\tau} \quad \text{with } R = \frac{n_0}{\tau} \tag{3}$$

In eqn (3), G_{BG} and R are the carrier generation rate (due to the background light) and recombination rate prior to t_0, respectively. Since steady-state is established for $t < t_0$, G_{BG} and R are equal. G is the additional carrier generation rate corresponding to the change in illumination at t_0. For $t \ll \tau$, the accumulation rate is constant and equals G. Accordingly, the observed linear charge carrier rise within the first 10 μs suggests that the free carrier loss due to recombination is not significant, consistent with the observed long τ for non-geminate recombination (Fig. S2, ESI†). As such, the carrier generation rate G can be estimated as a function of n_0 using the slope of the rise near t = 0 μs. To convert n_0 into V_{OP}, a second CE measurement is carried out,[31] this time with the device held at V_{OP} using a rheostat before switching to short-circuit (illuminated by green LED, 9.9 mW cm^{-2}). Fig. 2c shows the total extracted carriers as a function of initial steady-state V_{OP}. This result suggests that there is not a significant spatial reorganization of charge carriers between open-circuit and the operating condition as identical values of V_{OC} and V_{OP} correspond to similar carrier numbers, consistent with previous work in DTDCPB-C_{60} BHJ OPVs.[16] However, this equivalence of V_{OC} and V_{OP} may not generally hold across different active materials and device architectures, especially for the case of high intensity illumination (beyond 1 Sun).[16,27] With the relationship between n_0 and V_{OP}, the I_{Gen} can then be derived as a function of operating voltage as:

$$I_{Gen}(V_{OP}(n_0)) = e \cdot G(n_0) \tag{4}$$

Fig. 3a shows four representative plots of carrier number rise, the initial carrier number n_0 corresponds to V_{OP} = 48.4 mV, 102.7 mV, 142.7 mV and 200.0 mV. Additional carrier rise plots (V_{OP} = 241.2–799.9 mV) are show in Fig. S3 (ESI†).

A similar approach can also be used to experimentally measure I_{NGR} as a function of V_{OP}. The steady-state illumination is turned off at t_1 so that non-geminate recombination is the only pathway for carrier recombination. Fig. 3b shows four representative plots of carrier number decay for the DTDCPB-C_{60} BHJ ($n_0 = 8.35 \times 10^{10}$, 9.48×10^{10}, 1.05×10^{11}, 1.18×10^{11}). Additional carrier decay plots (corresponding to V_{OP} = 43.6–596.0 mV) are show in Fig. S4 (ESI†). In contrast to measuring the carrier lifetime with a perturbing laser pulse and calculating R as $\frac{n}{\tau}$, we measure R directly from the slope of the initial TPV decay.[16] The carrier discharging rate can be expressed as:

$$\frac{dn}{dt} = -\frac{n}{\tau} = -\left(R - \frac{n_0 - n}{\tau}\right) \tag{5}$$

For $t \ll \tau$, the value of R can be extracted from slope of the initial linear decay region. With this measured recombination rate and corresponding carrier number, the value of τ as a function of n can be extracted as $\frac{n}{R}$ (Fig. S2, (ESI†)). It should be noted that the carrier lifetime mentioned above is an effective lifetime for all charge carriers stored within the device. The shortest τ extracted here ($n = 1.31 \times 10^{11}$) is ~350 μs, corresponding to V_{OC} = 845.5 mV, which is much longer than the timescale for the measurement of G and R. Similar to I_{Gen} derived previously, I_{NGR} can be expressed as:

$$I_{NGR}(V_{OP}(n_0)) = e \cdot R(n_0) \tag{6}$$

With I_{Gen} extracted directly from the TPV measurement, the current loss from non-geminate recombination is the difference between I_{Gen} and the value of I_{Illum} collected from steady-state I–V characteristics. Fig. 4 shows I_{Gen} and I_{Illum} for a DTDCPB-C_{60} BHJ OPV illuminated by a green LED (9.9 mW cm^{-2}) as a function of voltage. While the measured I_{Gen} and I_{Illum} are well matched at low forward bias, the two curves begin to diverge at 0.4 V due to non-geminate recombination. This result suggests

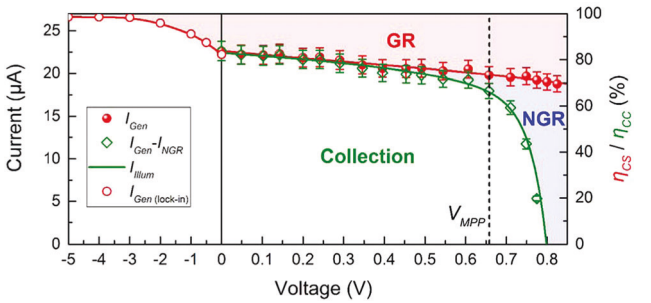

Fig. 4 Current from generated free carriers (I_{Gen}) and collected free carriers (I_{Illum}) as a function of voltage in the DTDCPB-C_{60} BHJ OPV of Fig. 1d under green LED illumination (9.9 mW cm^{-2}). The right axis shows the corresponding charge separation efficiency (η_{CS}) and charge collection efficiency (η_{CC}). The I_{Illum} recreated as $I_{Gen} - I_{NGR}$ from TPV measurements (green hollow diamond) is plotted for comparison with I_{Illum} extracted from I–V characteristics (green solid line). The red and blue areas represent illuminated current loss due to geminate recombination and non-geminate recombination, respectively. Under reverse bias, photocurrent (red hollow circle) is determined by a lock-in measurement. The photocurrent at −5 V is approximated as the maximum achievable current when charge recombination is fully eliminated.

that CT state dissociation is the only current-limiting process at short-circuit, while inefficient collection of free carriers causes a roll-off in I_{Illum} near V_{OC}, consistent with previous observations in solution-processed BHJ systems.[15,17,34] To further verify that I_{Illum} at short-circuit is limited primarily by geminate recombination, the I_{SC} was measured as a function of light intensity (simulated AM1.5G) (Fig. S5, ESI†). A linear dependence of I_{SC} on light intensity is observed, indicating the presence of a first order recombination process at short-circuit, consistent with geminate recombination.[35] While a free carrier collection efficiency of 100% at short-circuit seems counter-intuitive for a BHJ, the linear relationship between collected carriers and voltage near short-circuit suggests that the active layer capacitance is much lower than the electrode capacitance (Fig. 2c), leading to efficient carrier extraction and low non-geminate recombination loss within the mixed active layer.[16,36] To further check the reliability of this technique, the I_{Illum} recreated from the values of I_{Gen} and I_{NGR} measured directly from TPV is also plotted in Fig. 4. The recreated I_{Illum} is in excellent agreement with the measured I–V characteristics. We also accurately recreate I_{Illum} as a function of light intensity in Fig. S7 (ESI†).

To extract the absolute values of the η_{CS} and η_{CC} in eqn (2) as a function of voltage, the maximum possible current I_{Max} must also be known. Due to the near unity exciton diffusion efficiency (η_{Diff}) of an optimized BHJ, I_{Max} can be approximated as I_{Illum} at high reverse bias (−5 V), with both geminate and non-geminate recombination losses overcome by the large applied field.[20,29,37,38] For the DTDCPB-C_{60} BHJ device, $I_{Illum} \sim I_{Gen}$ (*i.e.* $I_{NGR} = 0$) under reverse bias, since the collection of free carriers is already efficient ($\eta_{FC} \approx 100\%$) at short-circuit. At short-circuit, the value of I_{Gen} obtained from the lock-in measurement (22.2 μA) is in good agreement with the value of I_{Gen} (22.6 μA) extracted using TPV. The value of I_{Gen} (lock-in) is plotted as a function of reverse bias in Fig. 4. This leads to a value of η_{CS} = 85.0% at short-circuit, consistent with the value extracted from reverse bias external quantum efficiency measurements (Fig. S8, ESI†).[20] At the maximum power point (660 mV), values of η_{CS} = 74.4% and η_{FC} = 88.9% are extracted, leading to an overall η_{CC} = 66.1%. For this device, both geminate and non-geminate recombination limit the power output at the maximum power point voltage (V_{MPP}), and CT state separation serves as the major limiting step to complete exciton-to-carrier conversion despite efficient exciton harvesting in the mixed active layer. Thus, there is still room for further improvement in η_{CS} in the DTDCPB-fullerene system, which has already been used to demonstrate high power conversion efficiency (8–10%).[32,33] Fig. S9 (ESI†) compares the photovoltage-extracted value of I_{Gen} to that obtained by subtracting the magnitude of the dark current from the illuminated current. The difference is found to underestimate the actual value of I_{Gen}.

While the discussion to this point is focused on BHJ OPVs, the photovoltage approach to measure I_{Gen} is widely applicable to OPVs with a variety of architectures. We further identify recombination losses in DTDCPB-C_{60} and CuPc-C_{60} planar heterojunction (PHJ) OPVs to elucidate what processes limit the FF in these devices. As η_{Diff} is no longer unity in a PHJ, I_{Max} cannot be approximated as the reverse bias I_{Gen}, as reverse bias may also improve η_{Diff} *via* bulk exciton ionization, leading to an overestimate of I_{Max}.[39] Therefore, optical modeling and a standard diffusion equation are generally used to estimate I_{Max} in a PHJ. This approach requires an accurate estimate of the exciton diffusion length in non-luminescent active materials like CuPc, nontrivial to determine experimentally.[18,21]

Fig. 5a and b show the I_{Gen} and I_{Illum} of DTDCPB and CuPc planar devices under green LED illumination (33.2 mW cm^{-2}), respectively. The illuminated current losses of these devices

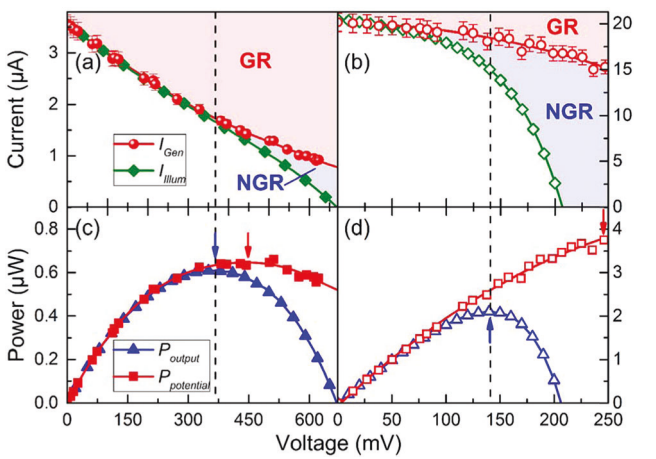

Fig. 5 (a and b) Current from generated free carriers and collected free carriers, (c and d) actual/potential power output as a function of voltage for DTDCPB-C_{60} (solid symbols) and CuPc-C_{60} (hollow symbols) planar OPVs in Fig. 1d under green LED illumination (33.2 mW cm^{-2}). The broken vertical line represents the voltage of maximum power point. The blue and red arrows show the maximum point of actual and potential power output, respectively.

due to geminate and non-geminate recombination are identified as a function of forward bias. Unlike the high FF (0.65) observed in BHJ devices, the DTDCPB-C_{60} PHJ shows a low FF of 0.26. This low FF comes from rapidly increased geminate recombination loss under forward bias. To better understand the origin of severe geminate recombination in DTDCPB-C_{60} PHJ under forward bias, we examine the impact of a neat DTDCPB layer on CT state separation in planar mixed heterojunction (PMHJ) devices (Fig. S10, ESI†). The results suggest that the neat DTDCPB layer reduces the electric field at the D–A interface, frustrating CT state dissociation (see ESI† for further discussion). At V_{MPP} (370 mV), over 99.7% of I_{Illum} loss relative to short-circuit is from geminate recombination. Thus, for the DTDCPB-C_{60} PHJ, the I_{Illum} at V_{MPP} can be improved only slightly if non-geminate losses are reduced. It is essential to suppress geminate recombination to effectively improve device efficiency. This contrasts with the previously discussed DTDCPB-C_{60} BHJ which will benefit from a reduction in either geminate or non-geminate recombination losses. As in DTDCPB PHJs, devices based on CuPc-C_{60} are also limited by a low FF ($\sim$0.49). The efficiency of a CuPc PHJ device is limited by both geminate and non-geminate recombination, in contrast to the DTDCPB PHJ device. A η_{FC} of only 81.0% is observed at the maximum power point in the CuPc device while the η_{FC} is near unity at the same point for DTDCPB. As such, the limiting recombination mechanism within the power generating quadrant can vary with both device architecture and D–A materials choice.

While significant efforts have been made to suppress non-geminate recombination and improve V_{OC} in OPVs, these efforts are only fruitful if the device is limited by non-geminate recombination.[40–43] Accordingly, understanding the potential power output ($P_{potential}$) in the absence of free carrier loss is essential before attempting to reduce non-geminate recombination for improved V_{OC}. Fig. 5c and d show the actual output power (P_{output}) and $P_{potential}$ of DTDCPB and CuPc PHJ devices. For the DTDCPB planar device, both P_{output} and $P_{potential}$ increase with forward bias up to the maximum power point (0.37 V) then start to roll off. This suggests that the efficiency can be improved only slightly by further suppression of non-geminate recombination. To effectively improve η_P, more efficient dissociation of CT states is required. In contrast, $P_{potential}$ for the CuPc planar device increases with forward bias up to 250 mV, with the maximum voltage limited only by the background light source. If non-geminate recombination could be completely avoided (before 250 mV), an increase of 25% in V_{OC} and 80% in η_P could be achieved. As such, the CuPc planar device can benefit from reduction of either geminate or non-geminate recombination.

Conclusions

We present a photovoltage-based technique to directly probe free carrier generation in an OPV at any operating voltage. For the D–A systems studied here, we apply this technique to quantitatively decouple geminate and non-geminate recombination losses within the power generating quadrant. Geminate recombination is found to be a significant factor limiting the device efficiency while the role of non-geminate recombination can vary with choice of active materials and device architecture. This deeper understanding of recombination will help to guide materials selection and device design in efforts for high efficiency.

Conflicts of interest

There are no conflicts to declare.

Acknowledgements

This work was supported by National Science Foundation (NSF) Solid State and Materials Chemistry (SSMC) under DMR-1307066 and DMR-1708177. The authors thank Dr James Holst at Sigma-Aldrich Corporation for synthesizing DTDCPB.

References

1 J. Zhao, Y. Li, G. Yang, K. Jiang, H. Lin, H. Ade, W. Ma and H. Yan, *Nat. Energy*, 2016, **1**, 15027.
2 Y. Liang, Z. Xu, J. Xia, S. T. Tsai, Y. Wu, G. Li, C. Ray and L. Yu, *Adv. Mater.*, 2010, **22**, E135–E138.
3 Y. H. Chen, L. Y. Lin, C. W. Lu, F. Lin, Z. Y. Huang, H. W. Lin, P. H. Wang, Y. H. Liu, K. T. Wong, J. Wen, D. J. Miller and S. B. Darling, *J. Am. Chem. Soc.*, 2012, **134**, 13616–13623.
4 S. M. Menke, W. A. Luhman and R. J. Holmes, *Nat. Mater.*, 2013, **12**, 152–157.
5 X. Che, X. Xiao, J. D. Zimmerman, D. Fan and S. R. Forrest, *Adv. Energy Mater.*, 2014, **4**, 1400568.
6 Y. He, H.-Y. Chen, J. Hou and Y. Li, *J. Am. Chem. Soc.*, 2010, **132**, 1377–1382.
7 S. H. Park, A. Roy, S. Beaupré, S. Cho, N. Coates, J. S. Moon, D. Moses, M. Leclerc, K. Lee and A. J. Heeger, *Nat. Photonics*, 2009, **3**, 297–302.
8 J. D. Chen, C. Cui, Y. Q. Li, L. Zhou, Q. D. Ou, C. Li, Y. Li and J. X. Tang, *Adv. Mater.*, 2015, **27**, 1035–1041.
9 H. Hu, K. Jiang, G. Yang, J. Liu, Z. Li, H. Lin, Y. Liu, J. Zhao, J. Zhang and F. Huang, *J. Am. Chem. Soc.*, 2015, **137**, 14149–14157.
10 Y. Liu, C.-C. Chen, Z. Hong, J. Gao, Y. M. Yang, H. Zhou, L. Dou, G. Li and Y. Yang, *Sci. Rep.*, 2013, **3**, 3356.
11 Y. Yang, Z.-G. Zhang, H. Bin, S. Chen, L. Gao, L. Xue, C. Yang and Y. Li, *J. Am. Chem. Soc.*, 2016, **138**, 15011–15018.
12 W. Zhao, D. Qian, S. Zhang, S. Li, O. Inganäs, F. Gao and J. Hou, *Adv. Mater.*, 2016, **28**, 4734–4739.
13 C. M. Proctor, M. Kuik and T.-Q. Nguyen, *Prog. Polym. Sci.*, 2013, **38**, 1941–1960.
14 D. Bartesaghi, I. del Carmen Pérez, J. Kniepert, S. Roland, M. Turbiez, D. Neher and L. J. A. Koster, *Nat. Commun.*, 2015, **6**, 7083.
15 D. Credgington, R. Hamilton, P. Atienzar, J. Nelson and J. R. Durrant, *Adv. Funct. Mater.*, 2011, **21**, 2744–2753.

16 D. Credgington, F. C. Jamieson, B. Walker, T. Q. Nguyen and J. R. Durrant, *Adv. Mater.*, 2012, **24**, 2135–2141.
17 C. G. Shuttle, B. O'Regan, A. M. Ballantyne, J. Nelson, D. D. Bradley and J. R. Durrant, *Phys. Rev. B: Condens. Matter Mater. Phys.*, 2008, **78**, 113201.
18 L. A. A. Pettersson, L. S. Roman and O. Inganas, *J. Appl. Phys.*, 1999, **86**, 487–496.
19 G. F. Burkhard, E. T. Hoke and M. D. McGehee, *Adv. Mater.*, 2010, **22**, 3293–3297.
20 R. Pandey and R. J. Holmes, *Appl. Phys. Lett.*, 2012, **100**, 083303.
21 S. M. Menke and R. J. Holmes, *Energy Environ. Sci.*, 2014, **7**, 499–512.
22 S. Albrecht, W. Schindler, J. Kurpiers, J. Kniepert, J. C. Blakesley, I. Dumsch, S. Allard, K. Fostiropoulos, U. Scherf and D. Neher, *J. Phys. Chem. Lett.*, 2012, **3**, 640–645.
23 K. Vandewal, S. Albrecht, E. T. Hoke, K. R. Graham, J. Widmer, J. D. Douglas, M. Schubert, W. R. Mateker, J. T. Bloking and G. F. Burkhard, *Nat. Mater.*, 2014, **13**, 63.
24 T. Zhang, H. Han, Y. Zou, Y.-C. Lee, H. Oshima, K.-T. Wong and R. J. Holmes, *ACS Appl. Mater. Interfaces*, 2017, **9**, 25418–25425.
25 V. Mihailetchi, J. Wildeman and P. Blom, *Phys. Rev. Lett.*, 2005, **94**, 126602.
26 L. Koster, M. Kemerink, M. M. Wienk, K. Maturová and R. A. Janssen, *Adv. Mater.*, 2011, **23**, 1670–1674.
27 C. Shuttle, R. Hamilton, B. O'Regan, J. A. Nelson and J. Durrant, *Proc. Natl. Acad. Sci. U. S. A.*, 2010, **107**, 16448–16452.
28 J. Kniepert, M. Schubert, J. C. Blakesley and D. Neher, *J. Phys. Chem. Lett.*, 2011, **2**, 700–705.
29 R. A. Marsh, J. M. Hodgkiss and R. H. Friend, *Adv. Mater.*, 2010, **22**, 3672–3676.
30 T. K. Mullenbach, I. J. Curtin, T. Zhang and R. J. Holmes, *Nat. Commun.*, 2017, **8**, 14215.
31 T. K. Mullenbach and R. J. Holmes, *Appl. Phys. Lett.*, 2015, **107**, 123303.
32 Y. Zou, J. Holst, Y. Zhang and R. J. Holmes, *J. Mater. Chem. A*, 2014, **2**, 12397.
33 O. L. Griffith, X. Liu, J. A. Amonoo, P. I. Djurovich, M. E. Thompson, P. F. Green and S. R. Forrest, *Phys. Rev. B: Condens. Matter Mater. Phys.*, 2015, **92**, 085404.
34 S. R. Cowan, A. Roy and A. J. Heeger, *Phys. Rev. B: Condens. Matter Mater. Phys.*, 2010, **82**, 245207.
35 C. Deibel, T. Strobel and V. Dyakonov, *Adv. Mater.*, 2010, **22**, 4097–4111.
36 J. Carr and S. Chaudhary, *Appl. Phys. Lett.*, 2012, **100**, 213902.
37 L. Onsager, *Phys. Rev.*, 1938, **54**, 554.
38 C. L. Braun, *J. Chem. Phys.*, 1984, **80**, 4157–4161.
39 Y. Zou and R. J. Holmes, *Adv. Energy Mater.*, 2015, **5**, 1500019.
40 Y. Zou and R. J. Holmes, *ACS Appl. Mater. Interfaces*, 2015, **7**, 18306–18311.
41 T. D. Heidel, D. Hochbaum, J. M. Sussman, V. Singh, M. E. Bahlke, I. Hiromi, J. Lee and M. A. Baldo, *J. Appl. Phys.*, 2011, **109**, 104502.
42 D. Bilby, J. Amonoo, M. E. Sykes, B. Frieberg, B. Huang, J. Hungerford, M. Shtein, P. Green and J. Kim, *Appl. Phys. Lett.*, 2013, **103**, 203902.
43 Y. Zhong, A. Tada, S. Izawa, K. Hashimoto and K. Tajima, *Adv. Energy Mater.*, 2014, **4**, 1301332.
44 Y. Zou and R. J. Holmes, *Appl. Phys. Lett.*, 2013, **103**, 138.